Electronic Supplementary Material (ESI) for Journal of Materials Chemistry A.

Hollow cobalt phosphide octahedral pre-catalysts with exceptionally high intrinsic catalytic activity for electro-oxidation of water and methanol

Junyuan Xu,[a] Yuefeng Liu,[b] Junjie Li,[a] Isilda Amorim,[a] Bingsen Zhang,[c] Dehua Xiong,[d] Nan Zhang,[a] Sitaramanjaneva Mouli Thalluri,[a] Juliana P. S. Sousa[a] and Lifeng Liu[a*]

[a] *International Iberian Nanotechnology Laboratory (INL), Av. Mestre Jose Veiga, 4715-330 Braga, Portugal.*

[b] *Dalian National Laboratory for Clean Energy, Dalian Institute of Chemical Physics, Chinese Academy of Sciences, 116023, Dalian, China.*

[c] *Shenyang National Laboratory for Materials Science and Institute of Metal Research, Chinese Academy of Sciences, 110016, Shenyang, China.*

[d] *State Key Laboratory of Silicate Materials for Architectures, Wuhan University of Technology, 430070, Wuhan, China.*

Experimental procedures

Reagents

$(CH_3COO)_2Co \cdot 4H_2O$, $NaH_2PO_2 \cdot xH_2O$, polyvinylpyrrolidone (MW = 40000), ethylene glycol, and oleylamine were purchased from Sigma-Aldrich, and RuO_2 (anhydrous) was acquired from Alfa Aesar. All reagents were used as received without further purification.

Synthesis of hollow CoP octahedrons (OCHs) and porous CoP nanospheres (NSs)

Initially, the CoO OCHs were prepared by a hydrothermal method. 200 mg of $(CH_3COO)_2Co \cdot 4H_2O$ was firstly dissolved in 40 mL of oleylamine. After continuously stirring for 3 h at room temperature, the solution was transferred to a 50 mL Teflon-lined stainless steel autoclave. The autoclave was then sealed and maintained at 180 °C for 24 h in an oven. After cooling down to room temperature, the solution was centrifuged at 7000 rpm and rinsed several times with ethanol-cyclohexane mixture (volume ratio, 1/4). The as-obtained CoO OCHs were dried in a vacuum oven at 60 °C for 6 h. The surface oxidation of CoO OCHs was performed in air at 300 °C, resulting in a $CoO@Co_3O_4$ core/shell structure. Subsequently, phosphorization was carried out at the same temperature using $NaH_2PO_2 \cdot xH_2O$ as the source of phosphorus and high-purity N_2 (99.999 %) as carrier gas to obtain CoO@CoP. Typically, 0.1 g of $CoO@Co_3O_4$ powders were loaded in a ceramic boat, with 1.0 g of $NaH_2PO_2 \cdot xH_2O$ placed 2 cm away from the $CoO@Co_3O_4$ powders at the upstream side. The boat was then put into a tube furnace, wherein high-purity N_2 (99.999 %) was purged at a flow rate of 800 SCCM for 1 h to remove air. Afterwards, the furnace was ramped to 300 °C at a rate of 5 °C min^{-1}, held at this temperature for 4 h, and then cooled down naturally to room temperature. A constant N_2 flow was maintained in the whole process. Finally, the hollow CoP OCHs were obtained by etching CoO@CoP (2.5 mg mL^{-1}) in 0.5 M HCl for 30 min.

Porous CoP NSs were prepared by phosphorization of Co-glycorate NS precursors. The Co-glycorate NSs were synthesized as follows: 750 mg of $(CH_3COO)_2Co \cdot 4H_2O$, 375 mg of polyvinylpyrrolidone and 60 mL of ethylene glycol were added into a 250 ml three-necked flask with rigious magnetic stirring for 3 h at room temperature.[S1] Then the reaction temperature was increased to 190 °C in 10 minutes. After 1 h reaction, the solution was naturally cooled down to room temperature. The product was centrifuged, rinsed with ethanol several times to remove the residual polyvinylpyrrolidone, and then dried in a vacuum oven at 60 °C for 6 h. The phosphorization was carried out using the same procedure as mentioned above.

Material characterization

Powder XRD experiments were conducted on a X'Pert PRO diffractometer (PANalytical) set at 45 kV and 40 mA, using Cu K_α radiation (λ = 1.541874 Å) and a PIXcel detector. Data were collected with the Bragg-Brentano configuration in the 2θ range of 10 – 90^o at a scan speed of 0.01 $^o s^{-1}$. The crystallinity of the hollow CoP OCHs and porous CoP NSs was analyzed using Highscore software (PANalytical) with a standard reference of Cryst50. The crystallinity of Cryst50 was firstly calibrated to 50% by altering the parameter of Constant Background, and then the crystallinity of the hollow CoP OCHs and porous CoP NSs was obtained accordingly (**Fig. S12**). XPS characterization was carried out on an ESCALAB 250 instrument with Al K_α X-rays (1489.6 eV). SEM examination was performed on a FEI Quanta 650 FEG microscope equipped with INCA 350 spectrometer (Oxford Instruments) for EDX. TEM, HRTEM and EDX elemental mapping studies were conducted on a probe-corrected transmission electron microscope operating at 200 kV (FEI Themis 60-300). TG-DSC analysis was done in air with a heating rate of 2 $^\circ$C min^{-1} (Mettler Toledo).

The morphology and composition of pre-catalysts after the OER and MOR stability tests were also examined by SEM, EDX and XPS, respectively. Before the examination, the carbon paper substrate loaded with the catalysts was immersed in deionized water for 2 h to get rid of the residual electrolyte, and then dried naturally in air.

Electrode preparation and electrocatalytic measurements

The catalyst ink was prepared by ultrasonically dispersing 5 mg of catalysts into 1 mL of ethanol containing 50 μL of Nafion solution (Sigma, 5 wt %). To prepare an electrode for catalytic tests, 100 μL of catalyst ink was loaded on a CP substrate with an exposed area of 1 cm^2, leading to a loading density of *ca.* 0.5 mg cm^{-2}. The electrode was then dried at room temperature naturally in air. All electrocatalytic tests were carried out in a three-electrode configuration at room temperature using a Biologic VMP-3 potentiostat/galvanostat. The catalyst-loaded carbon paper, Pt wire (for OER) or graphite (for MOR), and a saturated calomel electrode (SCE) were utilized as working, counter and reference electrodes, respectively. The SCE reference was calibrated prior to each measurement in H_2-saturated 0.5 M H_2SO_4 solution using a clean Pt wire as the working electrode.

OER in 1.0 M KOH: The potentials are reported versus RHE in OER by converting the measured potentials according to the following equation:

$$E_{RHE} = E_{SCE} + 0.059 \times pH + 0.244 \quad \text{(S1)}$$

Cyclic voltammetry (CV) was performed at a scan rate of 5 mV s^{-1} in the potential range of 1.0 to 1.7 V *vs.* RHE. An *iR*-correction (85 %) was made to compensate the voltage drop between the reference and working electrodes, which was measured by a single-point high-frequency impedance measurement. EIS measurements were carried out at 1.49 V *vs.* RHE in the frequency range of 10^5 to 0.01 Hz with a 10 mV sinusoidal perturbation. The double layer

capacitance (C_{dl}) of the catalysts was estimated by performing CV at different scan rates (v) of 10, 20, 30, 40, 50, 60, 70, 80, 90 and 100 mV s^{-1}, followed by extracting the slope from the resulting $|j_a-j_c|/2$ *vs.* v plots, where j_a and j_c represent the anodic and cathodic currents at a given potential, respectively. The electrochemically-accessible surface area (ECSA) can be calculated by dividing the measured C_{dl} by the capacitance of a model catalyst over a unit surface area (usually 0.04 mF cm_{geo}^{-2}, according to previous report[S2]):

$$ECSA = C_{dl} / 0.04 \text{ mF cm}^{-2} \quad \text{(S2)}$$

The TOF_{mass} values were calculated through the following equation:[S3]

$$\text{TOF } (s^{-1}) = (j \times A) / (4 \times F \times n) \quad \text{(S3)}$$

where j (A cm^{-2}) is the current density at a given overpotential, A = 1.0 cm^2 is the geometric surface area of the working electrode, F = 96500 C mol^{-1} stands for the Faraday constant, n (mol) is mole number of transition metal(s) loaded on the electrode. All metal cations were assumed to be catalytically active, so the calculated value represents the lower limits of TOF. For hollow CoP OCHs and porous CoP NSs, the Co content (P_{Co}, in wt %) in the pre-catalysts was determined by inductively-coupled plasma mass spectroscopy (ICP-MS, Agilent 7700X). Specifically, 20 mg of pre-catalysts were dispersed in 12 g of concentrated nitric acid in an autoclave, which was then kept in an electric oven at 180 °C for 12 h. Subsequently, the acidic solution was diluted in a 50 mL volumetric flask. The analyses were done three times using *ca.* 10 mL solution each time to obtain an average value (P_{Co} = 62 wt % Co for hollow CoP OCH; P_{Co} = 61 wt % Co for porous CoP NSs). The n_{Co} was then obtained according to the following equation:

$$n_{Co} = \frac{0.0005\ g\ cm^{-2} \times 1.0\ cm^2 \times P_{Co}}{M_{Co}} \quad \text{(S4)}$$

where M_{Co} = 58.93 g mol^{-1} is the molecular weight of Co.

the calculation TOF_{mass} of commercial RuO_2 NPs is similar but n_{Ru} was obtained according to the following equation:

$$n_{Ru} = \frac{0.0005\ g\ cm^{-2} \times 1.0\ cm^2}{M_{RuO2}} \quad \text{(S5)}$$

where M_{RuO2} = 133.07 g mol^{-1} is the molecular weight of RuO_2.

The $TOF_{surface}$ values were calculated based on the number of active sites for each catalyst using the same formula as shown in **Equation S3**, but *n* in this case represents the number of surface active sites, namely surface charge (in the unit of C), which can be quantified through CV measurements in neutral solution (all electrochemically-accessible surface sites including those that are catalytically inactive, are taken into accunt. Therefore, thus-calculated TOF value represents the lower limit of $TOF_{surface}$). All CV measurements were conducted in the potential range of 0 – 0.6 V *vs.* RHE at a fixed scan rate of 50 mV s^{-1} in PBS solution (pH =7). The surface charge was then calculated as follows:[S4,S5]

$$Q_S = \frac{1}{2}\int_{E_0}^{E_1} \frac{j}{v}\, dE \quad \text{(S6)}$$

where *j* is the current density, *v* is the scan rate, and E_0 and E_1 represent the lower and upper potential limits, respectively.

The catalytic stability of all catalysts was assessed at a constant current density of 10 mA cm^{-2} in 1.0 M KOH solution at room temperature.

MOR in 1.0 M KOH + 1.0 M methanol: *iR*-corrected (85 %) CV was recorded at a scan rate of 5 mV s^{-1} in the potential range of 0 – 0.44 V *vs.* SCE. EIS measurements were carried out at 0.35 V *vs.* SCE in the frequency range of 10^5 – 0.01 Hz with a 10 mV sinusoidal perturbation.

The stability was examined by continuous CV scans in the potential range of 0 – 0.35 V *vs.* SCE at 100 mV s^{-1}. After a given number of CV cycles, the *iR*-corrected (85 %) CV (0 – 0.44 V *vs.* SCE, 5 mV s^{-1}) and EIS (0.35 V *vs.* SCE) were recorded, and the current density at 0.44 V *vs.* SCE and the R_{ct} value extracted from EIS were obtained and compared to the initial values.

Supporting figures and tables

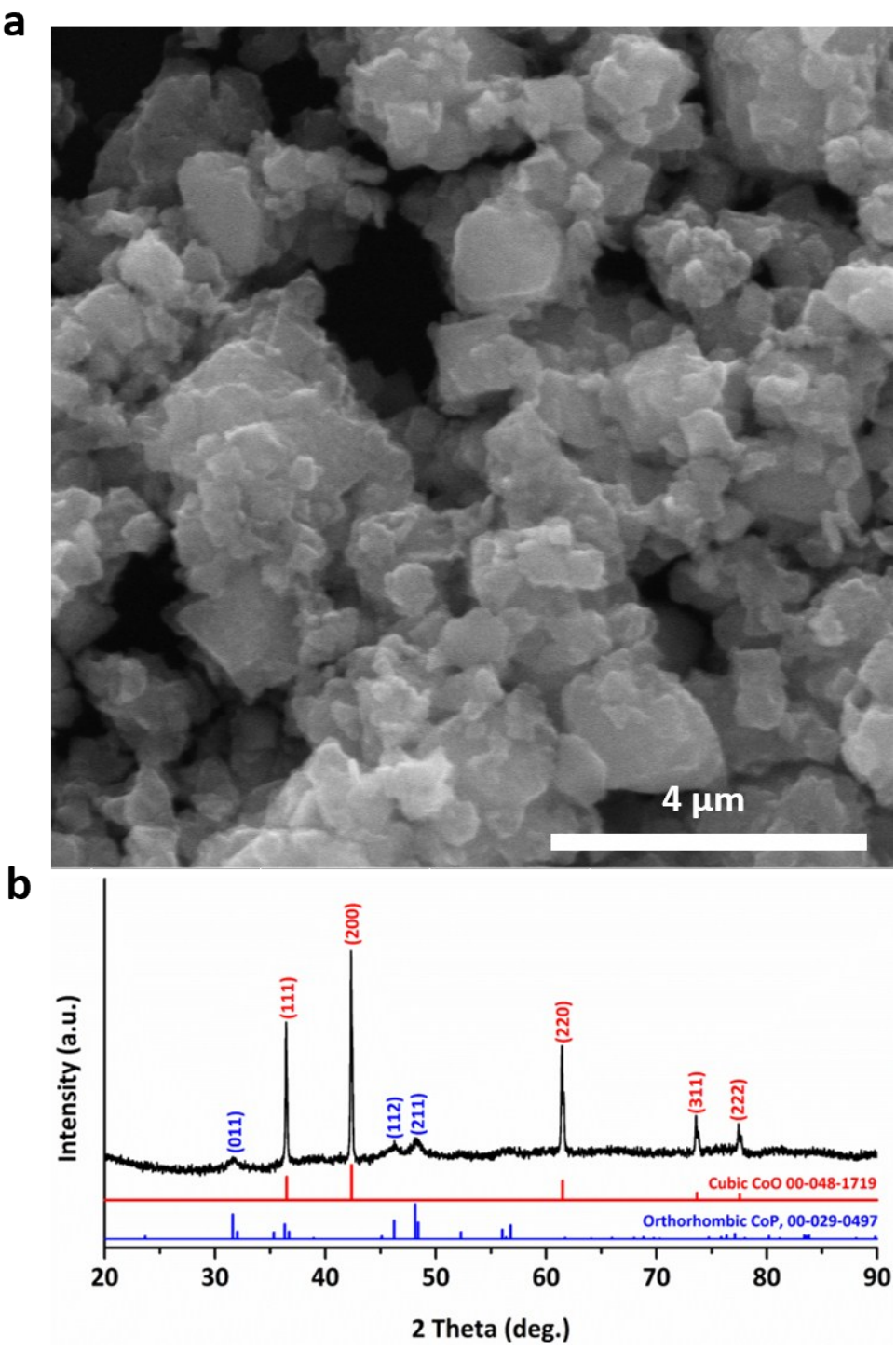

Fig. S1. (a) The morphology and (b) XRD pattern of CoO@CoP obtained by direct phosphorization of CoO OCHs at 300 ˚C in N_2 (99.999%) for 4 h.

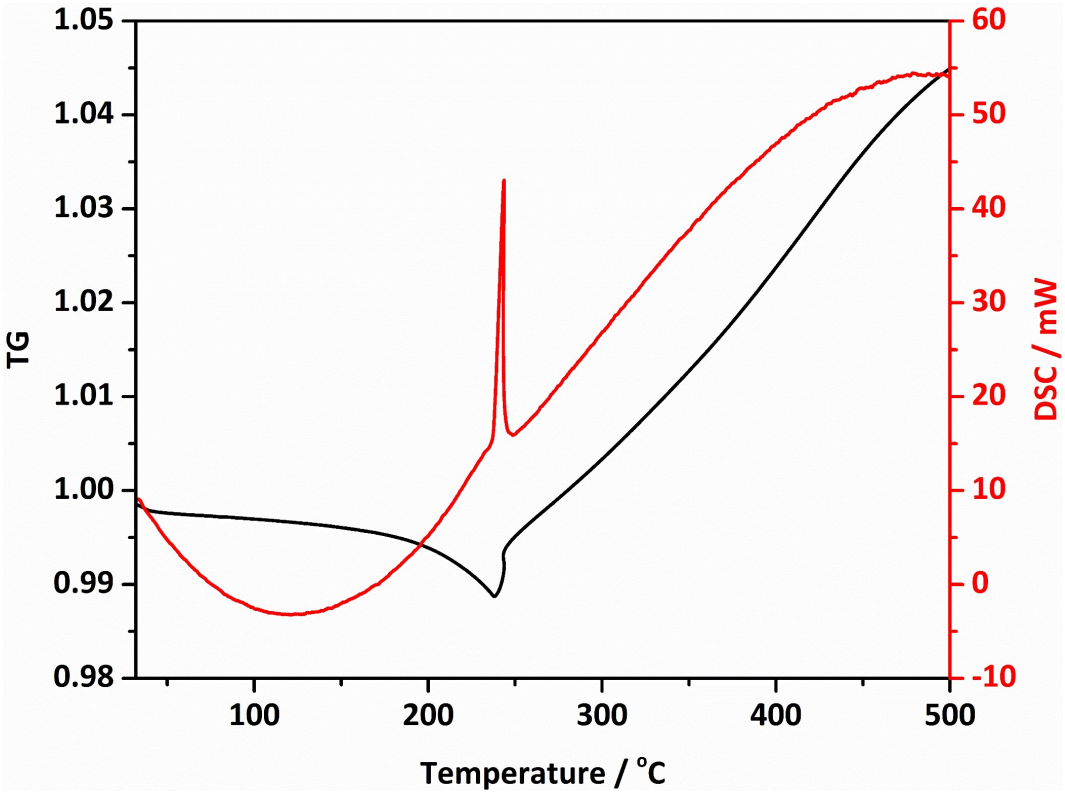

Fig. S2. TG-DSC curves of CoO OCHs recorded in air with a ramping rate of 2 ˚C min^{-1}.

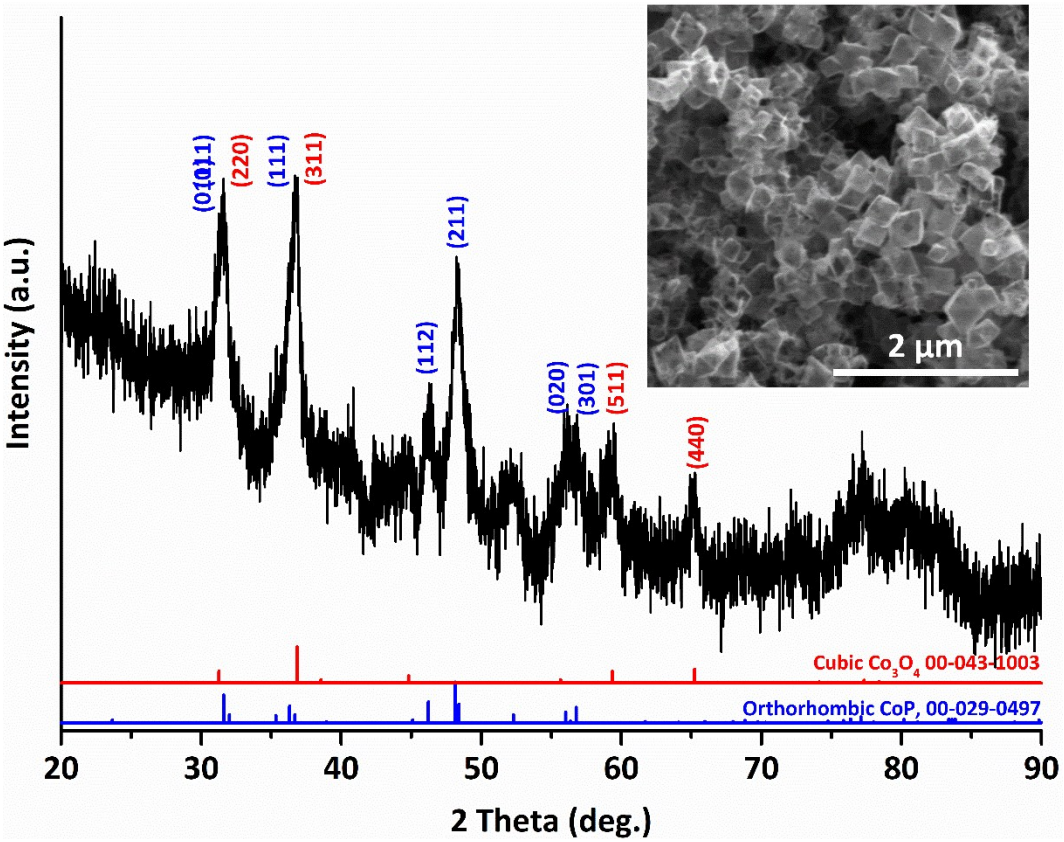

Fig. S3. XRD pattern of the CoP sample prepared by post annealing of CoO OCHs in air at 350 ˚C for 2 h, followed by the same phosphorization and chemical etching processes as those used for preparing hollow CoP OCHs. In addition to the diffractions from CoP, XRD peaks from Co_3O_4 are also observed, indicating incomplete conversion of Co_3O_4 to CoP. The standard powder diffraction patterns of cubic Co_3O_4 (ICDD No.00-043-1003) and orthorhombic CoP (ICDD No. 00-029-0497) are given for reference. The inset shows the morphology of the sample, which also exhibits hollow structure.

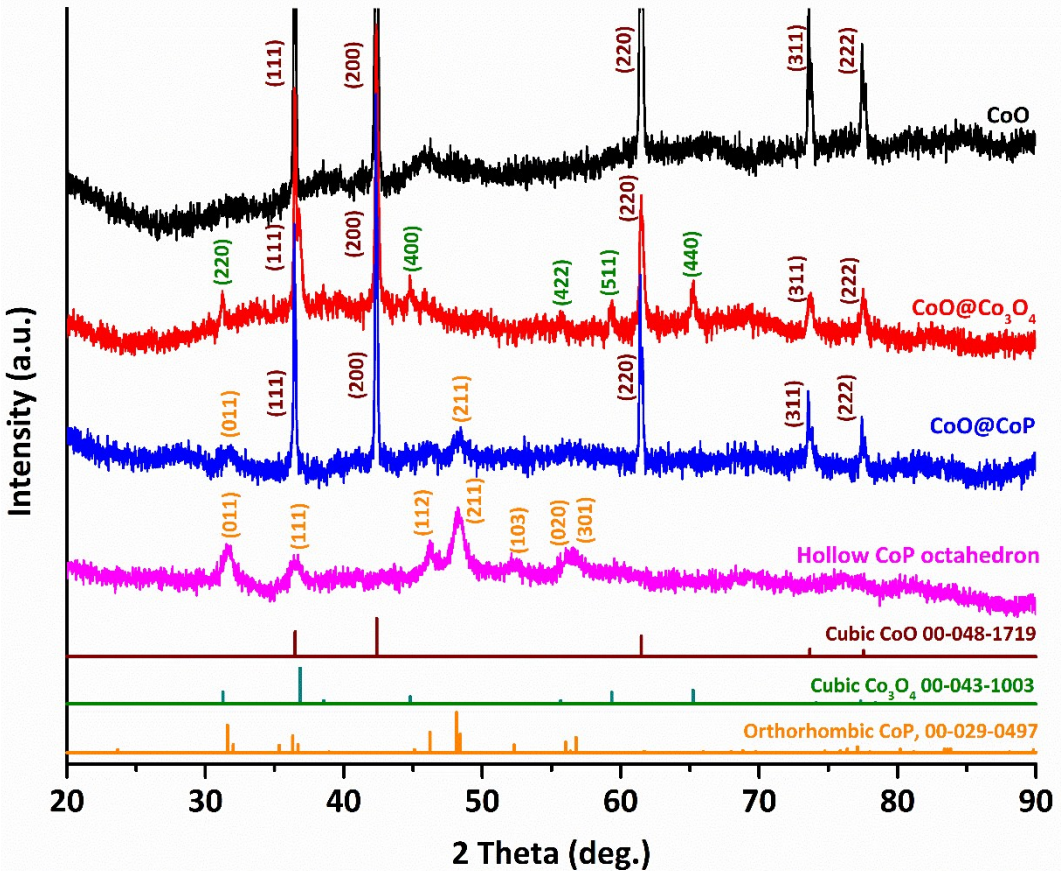

Fig. S4. XRD patterns of CoO, CoO@Co_3O_4, CoO@CoP and hollow CoP OCH pre-catalysts. The standard powder diffraction patterns of cubic CoO (ICDD No.00-048-1719), cubic Co_3O_4 (ICDD No.00-043-1003) and orthorhombic CoP (ICDD No. 00-029-0497) are given for reference.

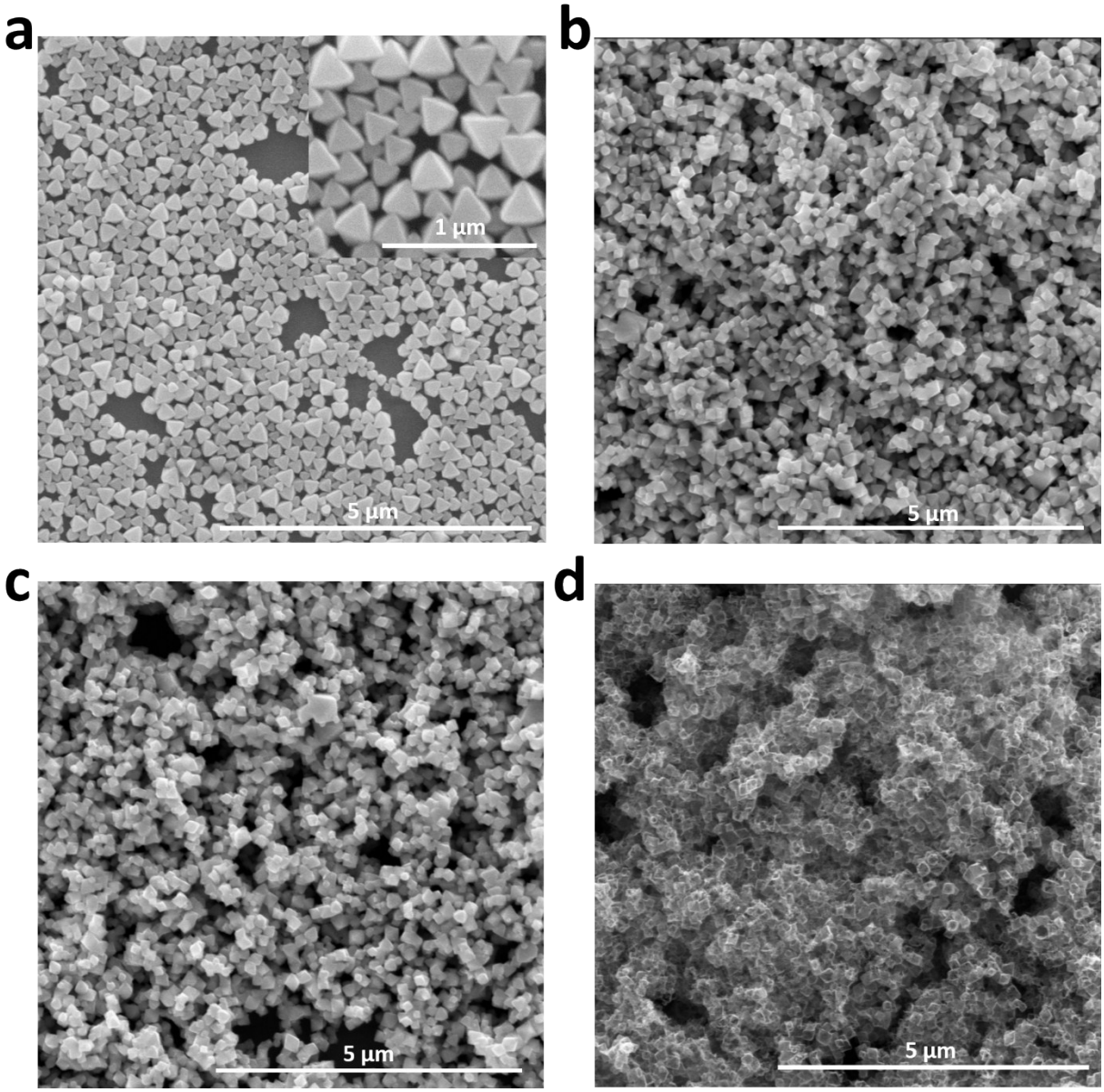

Fig. S5. SEM images showing the morphology of (a) CoO, (b) CoO@Co_3O_4, (c) CoO@CoP and (d) Hollow CoP OCHs.

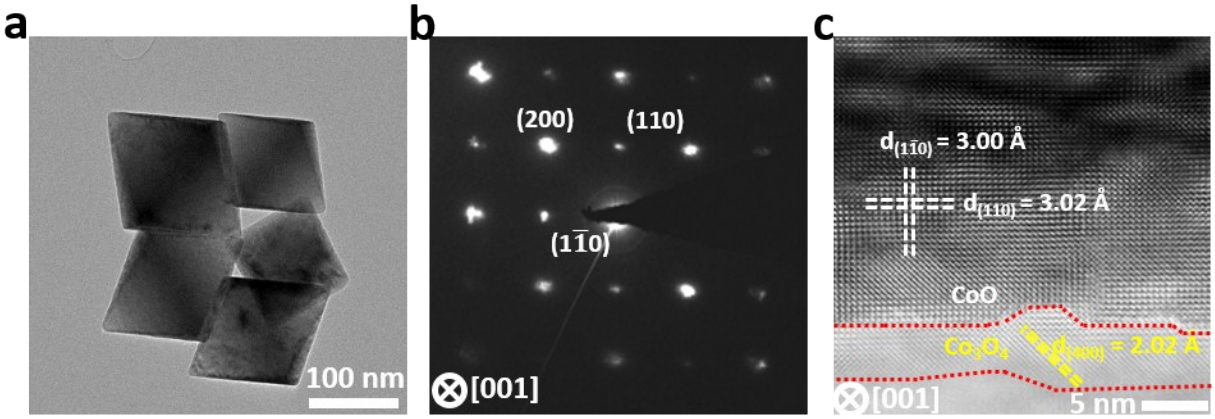

Fig. S6. TEM characterization of CoO@Co_3O_4 OCHs.

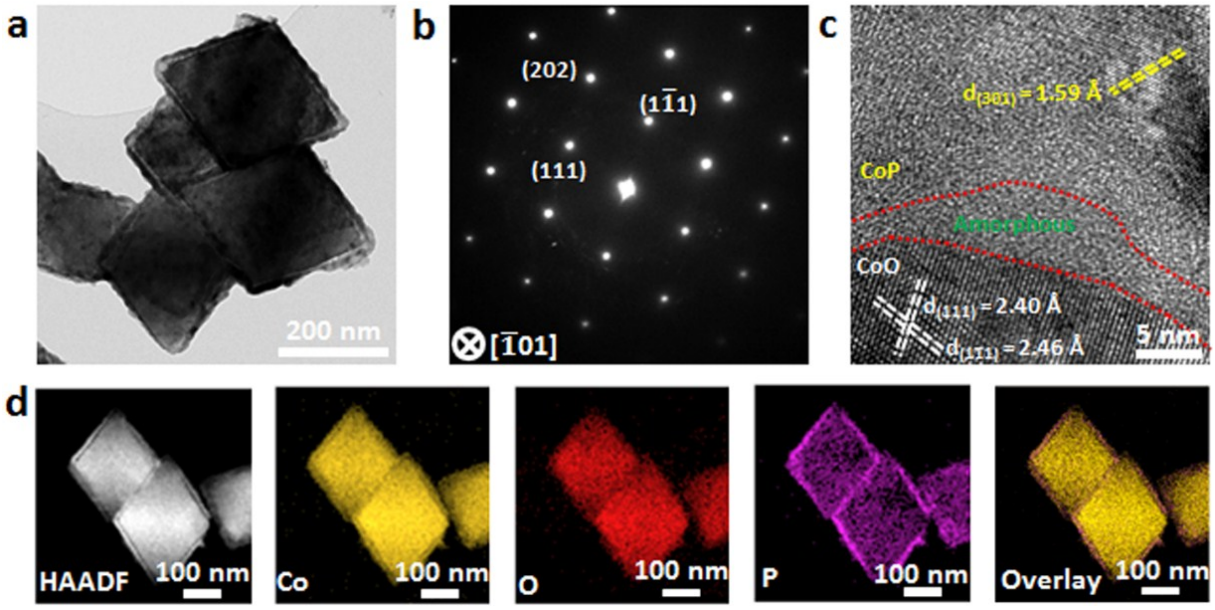

Fig. S7. TEM characterization of CoO@CoP OCHs.

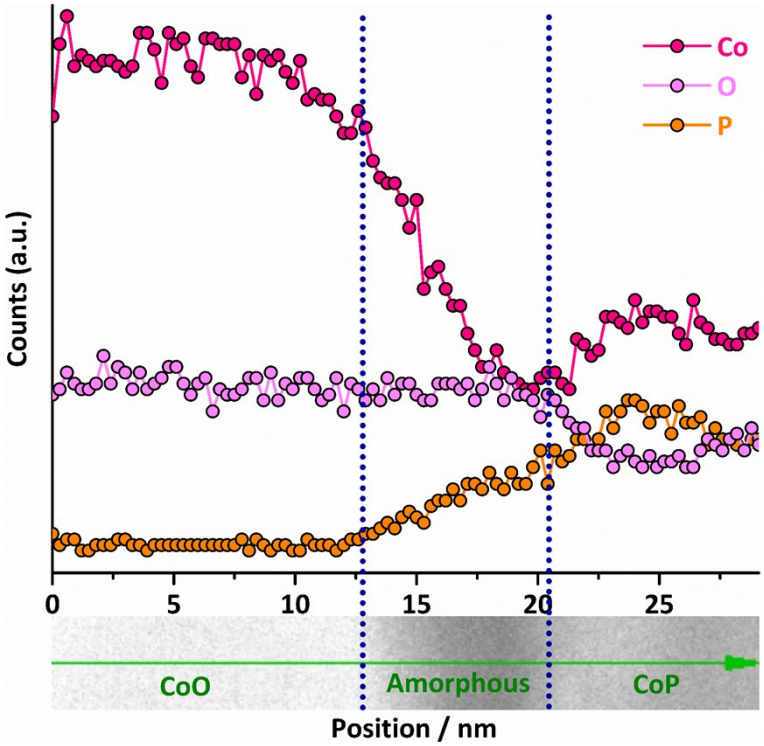

Fig. S8. TEM-EDX line scan over a single CoO@CoP OCH.

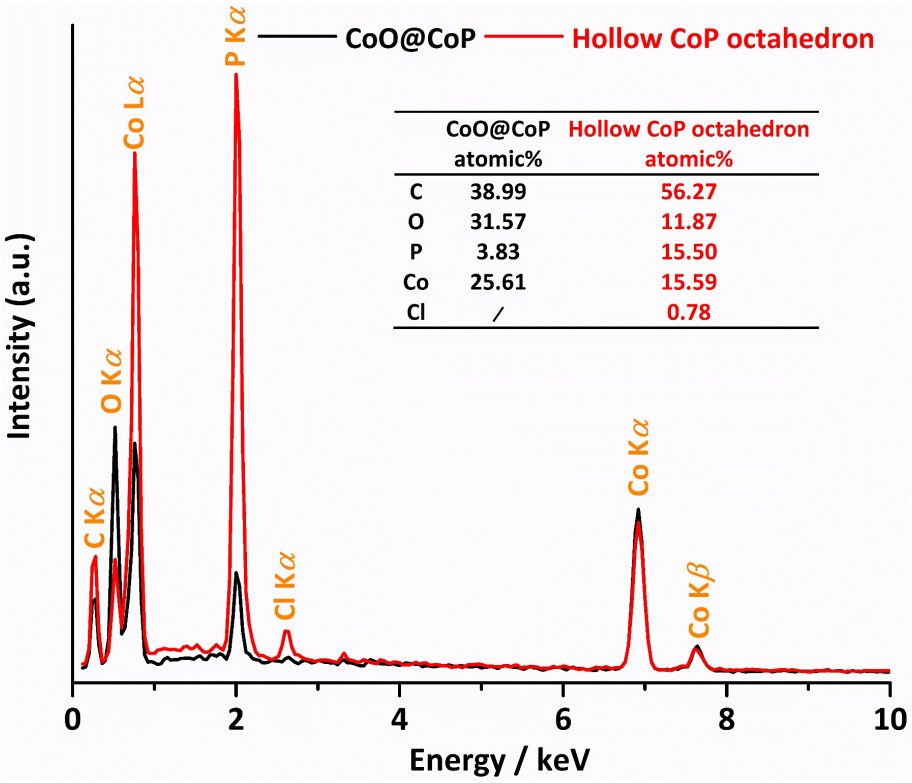

Fig. S9. EDX spectra of CoO@CoP and hollow CoP OCHs.

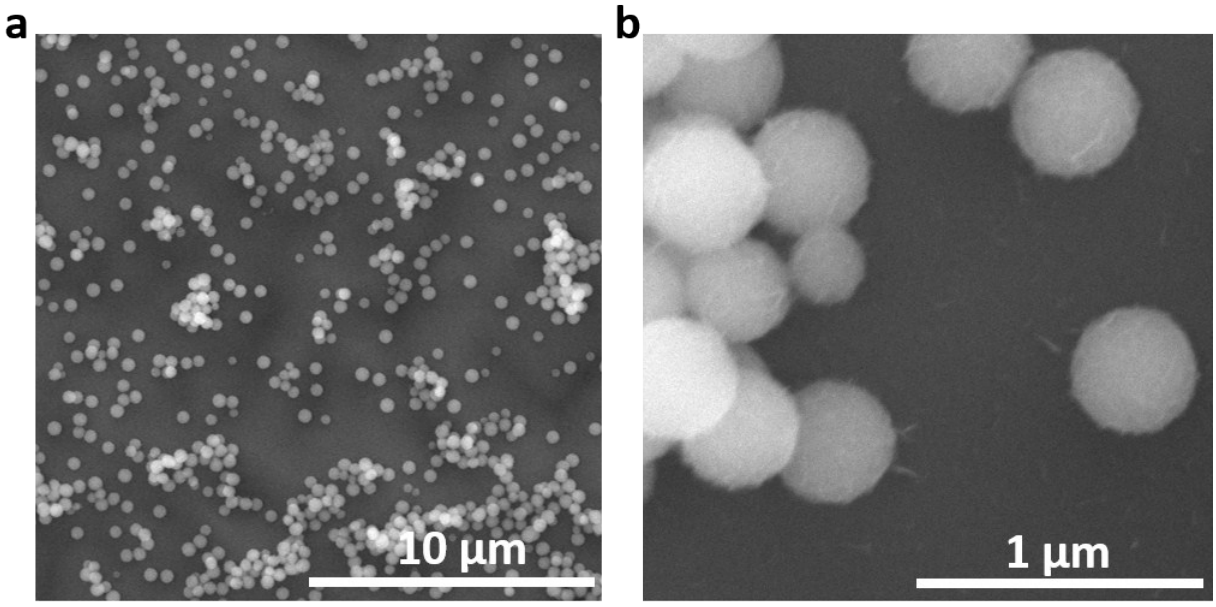

Fig. S10. SEM images showing the morphology of the Co-glycorate NS precursors. (a) Low-magnification and (b) high-magnification micrographs.

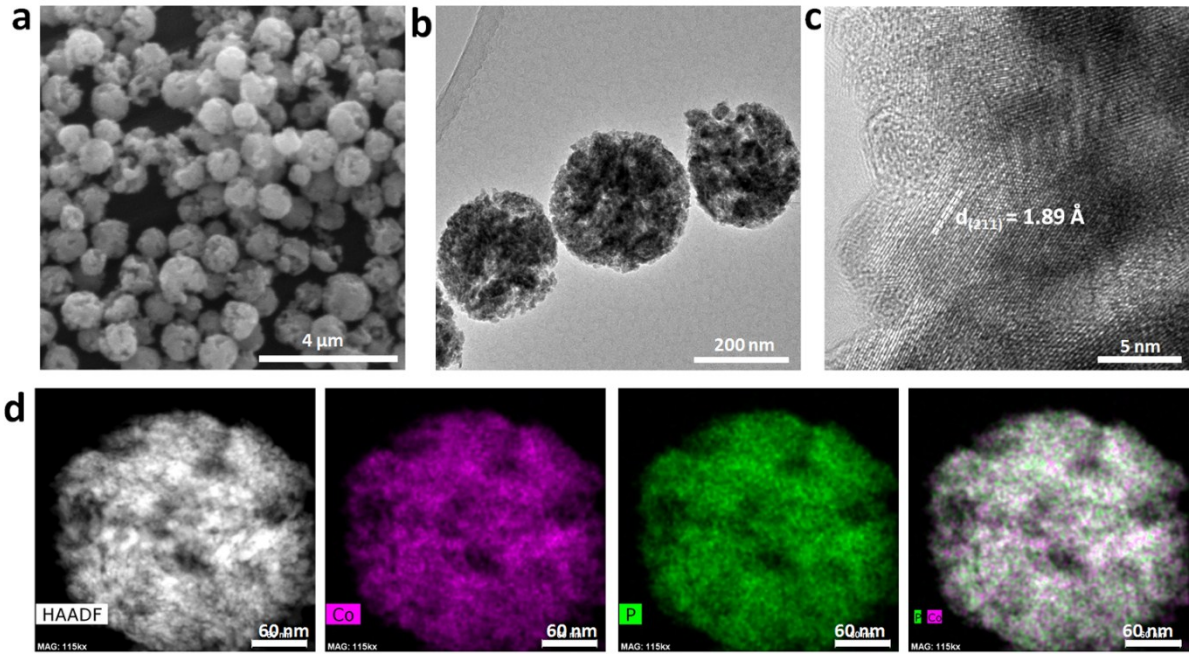

Fig. S11. Morphological, microstructural and compositional characterization of porous CoP NSs. (a) SEM image. (b) TEM, (c) HRTEM and (d) HAADF-STEM images and elemental maps of Co, P and their overlay.

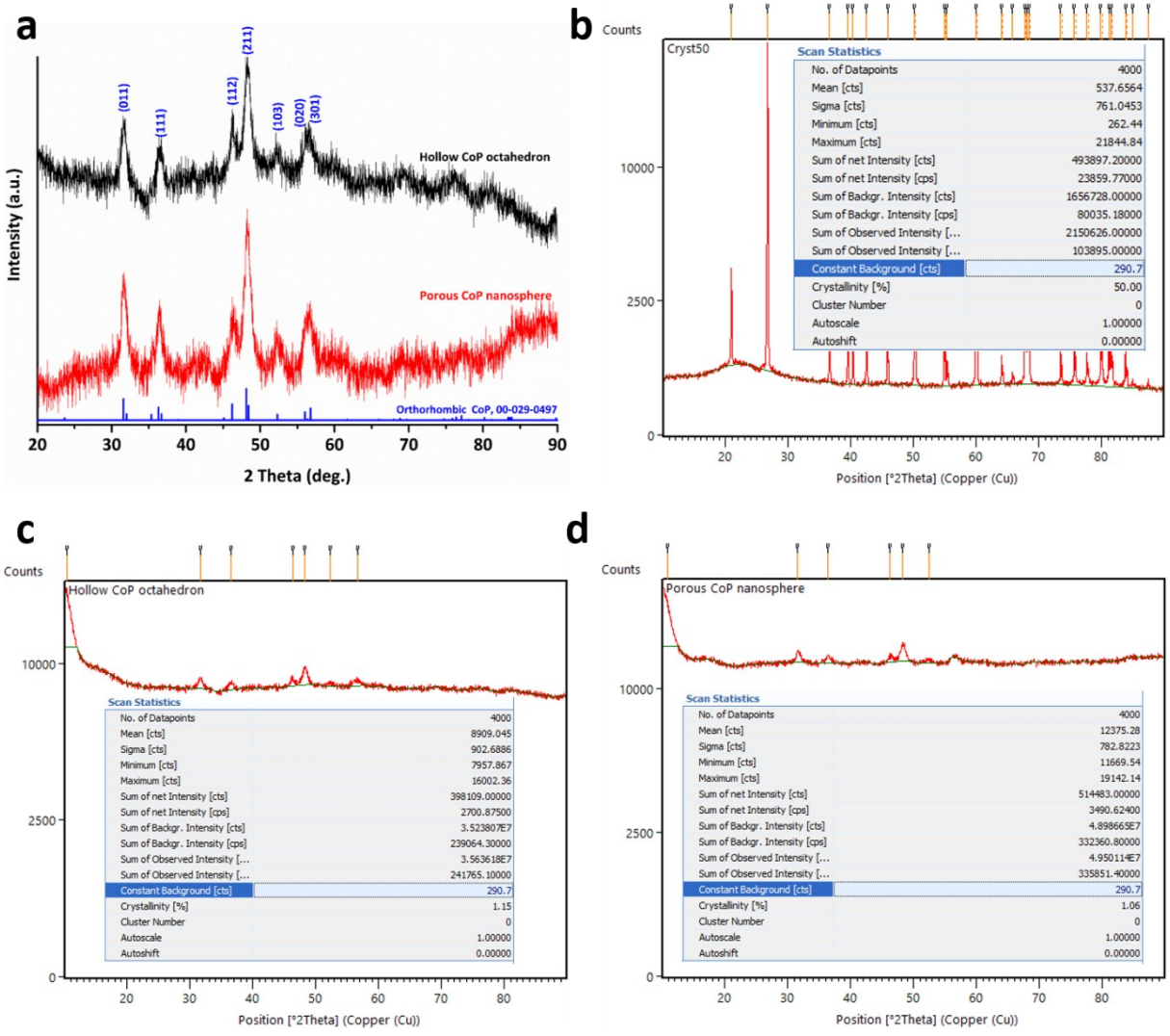

Fig. S12. (a) XRD patterns of hollow CoP OCH and porous CoP NS pre-catalysts. The standard powder diffraction pattern of orthorhombic CoP (ICDD No. 00-029-0497) is given for reference. (b) XRD pattern of the crystallinity calibration reference Cryst50. Crystallinity data of (c) Hollow CoP OCHs and (d) porous CoP NSs.

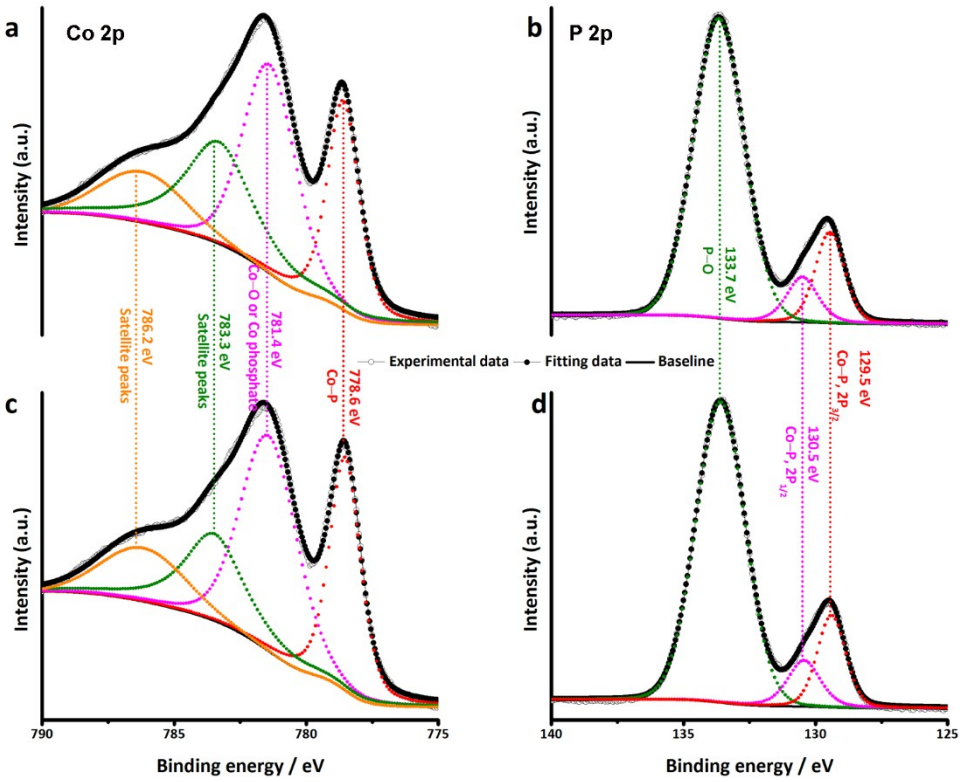

Fig. S13. (a) Co 2p and (b) P 2p XPS spectra of hollow CoP OCHs. (c) Co 2p and (d) P 2p XPS spectra of porous CoP NSs.

Fig. S13a and S13c are the high-resolution Co $2p_{3/2}$ XPS spectra of hollow CoP OCHs and porous CoP NSs, respectively. Peak deconvolution shows two main peaks at 778.6 and 781.4 eV and two satellite peaks at 783.3 and 786.2 eV.[S6,S7] The characteristic binding energy (BE) peak at 778.6 eV generally relates to the Co 2p contribution of cobalt phosphides, which is a good indication of Co–P bond formation; while the BE peak at 781.4 eV may be associated with the oxidized Co species that likely result from the slight surface oxidation, as commonly observed in other transition metal phosphides.[S3,S8-S10] As far as the P 2p spectra are concerned (Fig. 13b and S13d), two BE peaks appear at 129.5 and 130.5 eV, which can be assigned to the low-valence P and the $2p_{3/2}$ and $2p_{1/2}$ core levels of central P atoms in phosphide, respectively,[S6-S11] confirming the formation of Co–P bonds. The peak located at 133.7 eV is assigned to P–O bonding, which should originate from surface oxidation upon exposing the samples to air.[S3,S6-S11]

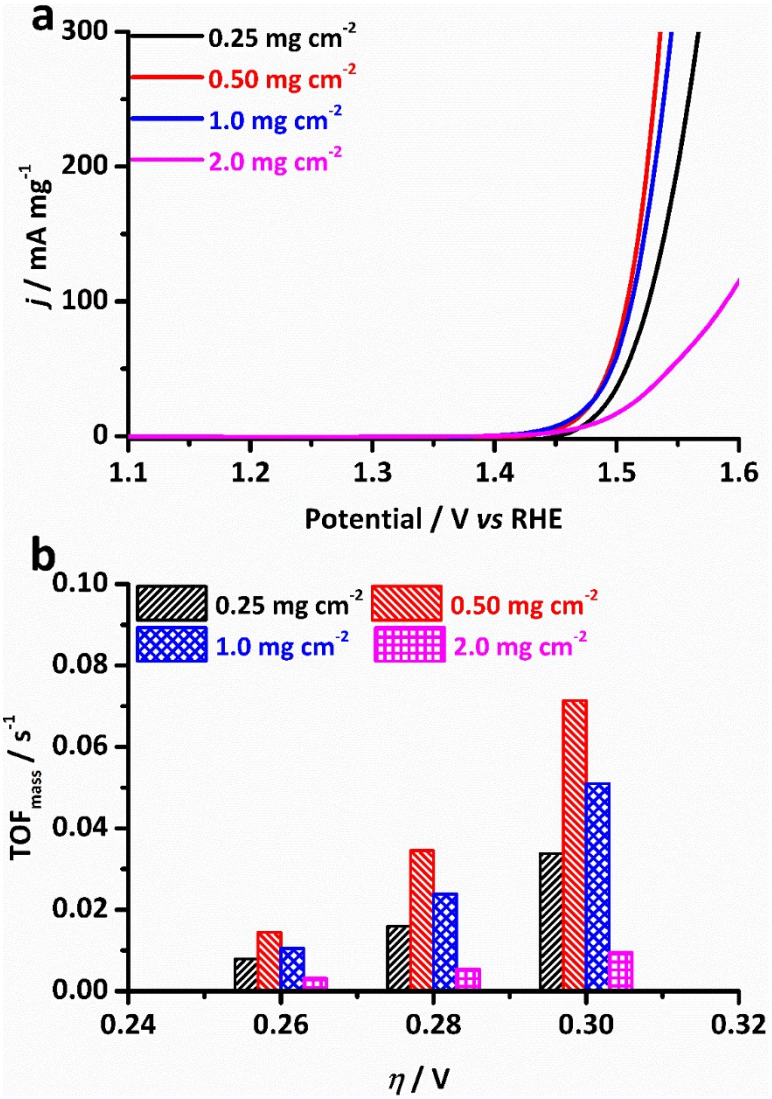

Fig. S14. (a) Mass activity of hollow CoP OCHs with different loadings. (b) Mass-based TOF values of hollow CoP OCHs with different loadings calculated at η = 260, 280 and 300 mV.

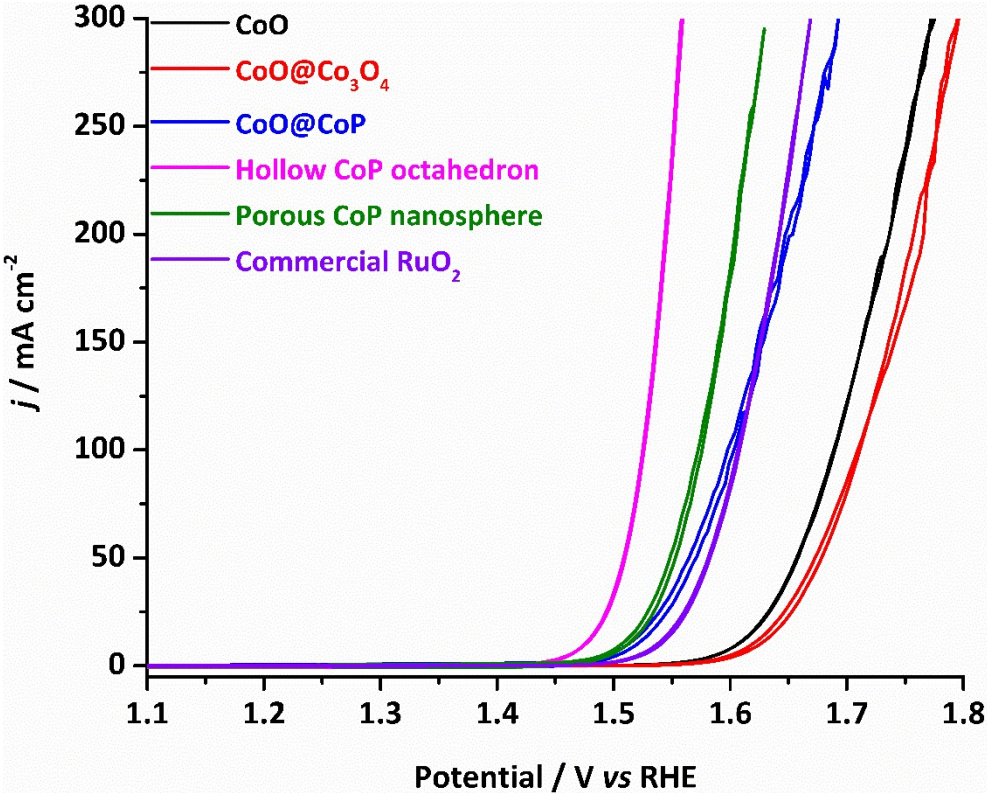

Fig. S15. The *iR*-corrected CV curves of CoO, CoO@Co_3O_4, CoO@CoP, hollow CoP OCHs, porous CoP NSs and commercial RuO_2 NPs recorded after pre-activation.

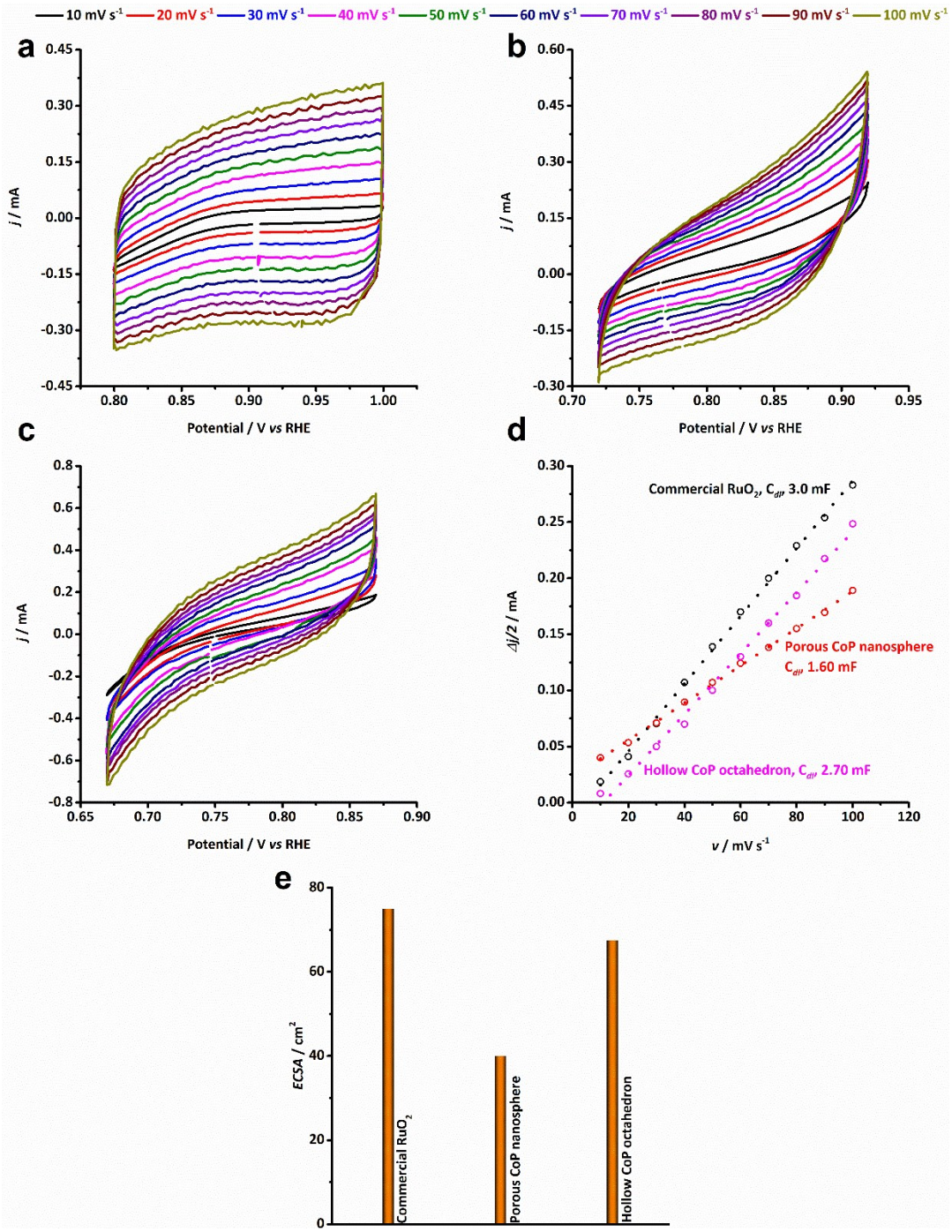

Fig. S16. Electrochemical CV curves of (a) commercial RuO_2 NP, (b) porous CoP NS and (c) hollow CoP OCH pre-catalysts recorded at different scan rates of 10, 20, 30, 40, 50, 60, 70, 80, 90 and 100 mV s^{-1}. (d) Plots of the capacitive currents as a function of the scan rate for all pre-catalysts. (e) ECSAs of all pre-catalysts.

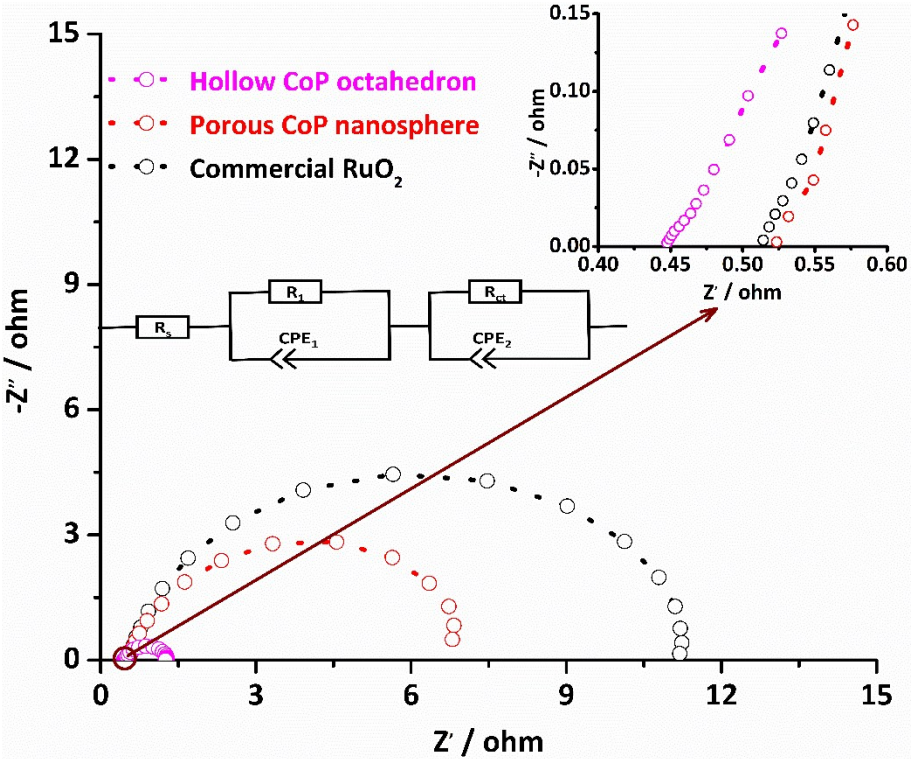

Fig. S17. The Nyquist plots of hollow CoP OCH, porous CoP NS and commercial RuO_2 NP pre-catalysts measured at 1.49 V *vs* RHE. The scattered open circles are experimental data and the dotted lines are fitting curves. The insets show the zoomed view of the plots in the high frequency regions (top) and the equivalent circuit model used for fitting (middle). R_s and R_{ct} represent the equivalent series resistance and charge transfer resistance, respectively. CPE stands for the constant phase element.

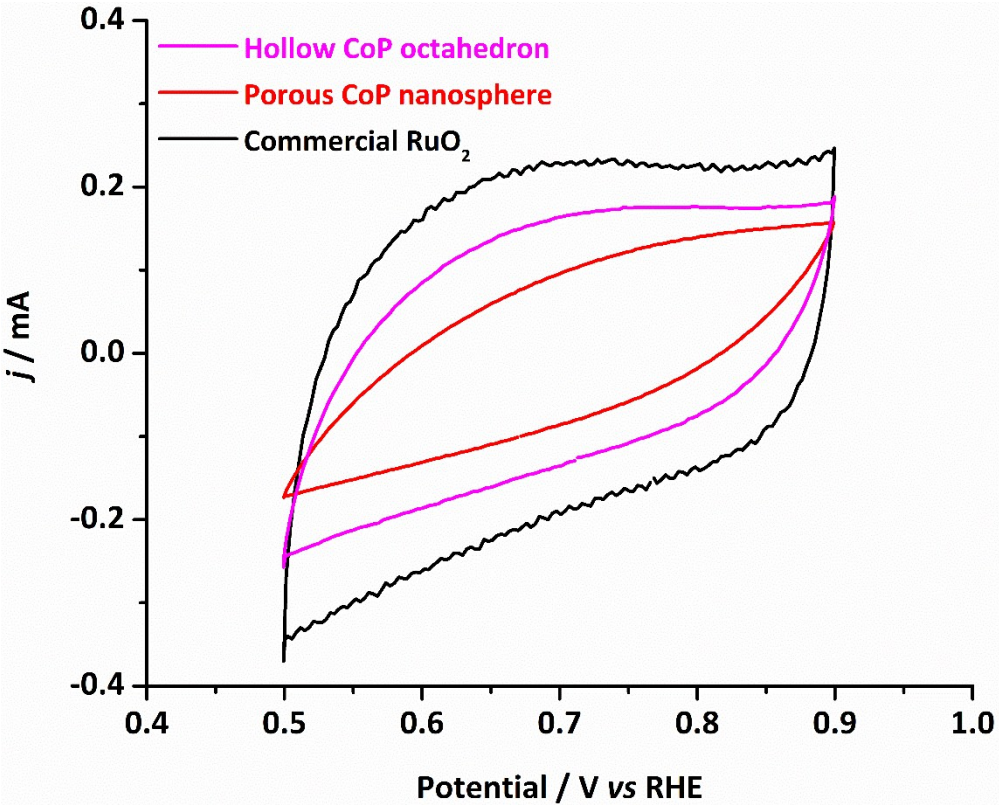

Fig. S18. CVs of hollow CoP OCH, porous CoP NS, and commercial RuO_2 NP pre-catalysts measured in PBS solution (pH = 7) at 50 mV s^{-1}. The surface charges are 2170, 1520, and 3090 μC for hollow CoP OCHs, porous CoP NSs, and commercial RuO_2 NPs, respectively.

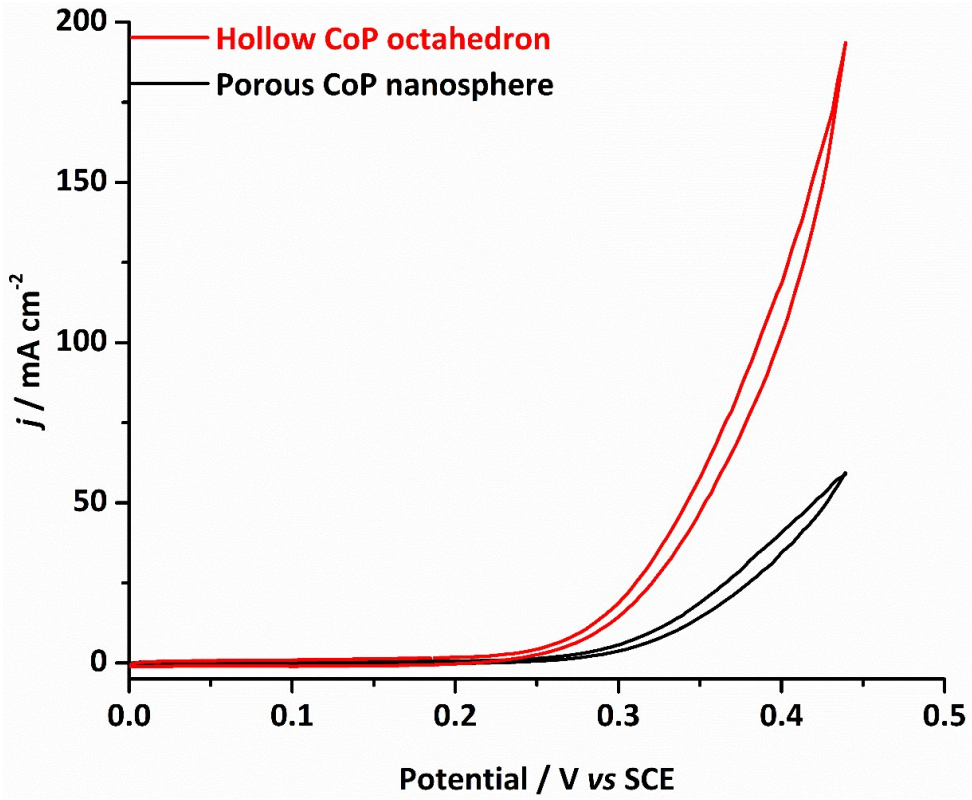

Fig. S19. *iR*-corrected CV curves of hollow CoP OCH and porous CoP NS pre-catalysts measured in 1.0 M KOH and 1.0 M methanol.

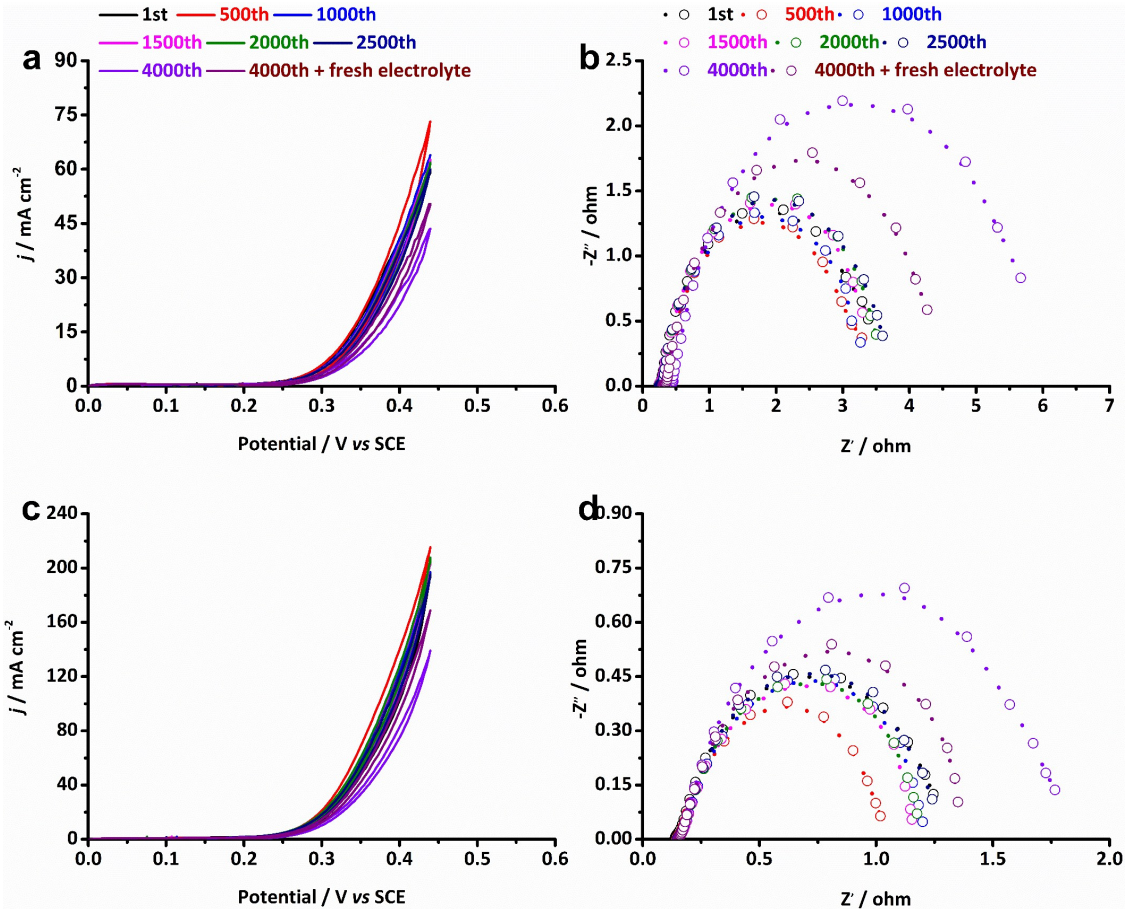

Fig. S20. (a) *iR*-corrected CV curves recorded at a scan rate of 5 mV s^{-1} and (b) Nyquist plots measured at 0.35 V *vs.* SCE in 1.0 M KOH + 1.0 M methanol for porous CoP NSs after different voltammetry cycles in the potential range of 0 – 0.35 V *vs.* SCE at a scan rate of 100 mV s^{-1}. (c) *iR*-corrected CV curves recorded at a scan rate of 5 mV s^{-1} and (d) Nyquist plots measured at 0.35 V *vs.* SCE in 1.0 M KOH + 1.0 M methanol for hollow CoP OCHs after different voltammetry cycles in the potential range of 0 – 0.35 V *vs.* SCE at a scan rate of 100 mV s^{-1}.

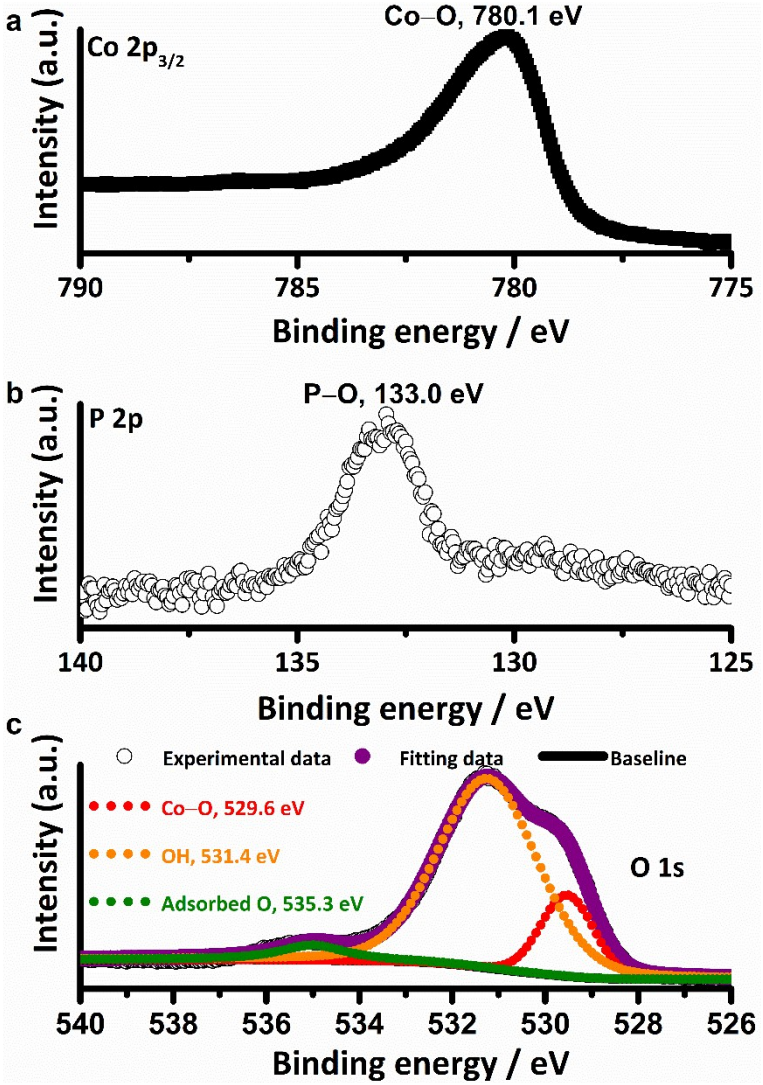

Fig. S21. (a) Co $2p_{3/2}$, (b) P 2p and (c) O 1s XPS spectra of hollow CoP OCHs after the OER test at 10 mA cm^{-2} for 60 h.

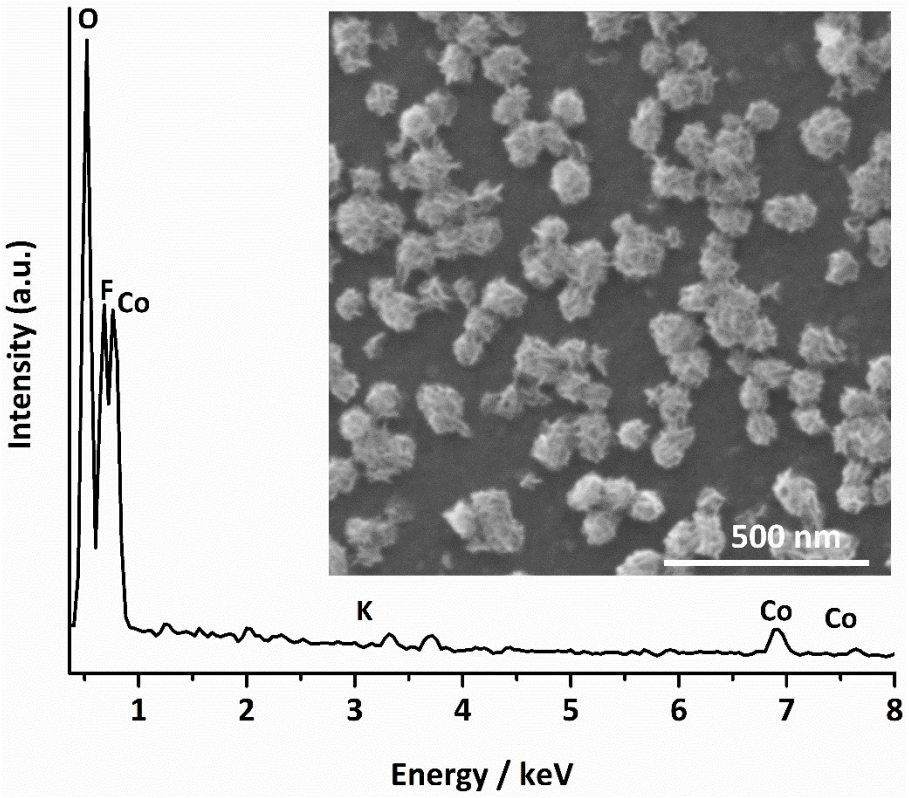

Fig. S22. SEM image and EDX spectrum of hollow CoP OCHs after the OER test at 10 mA cm^{-2} for 60 h.

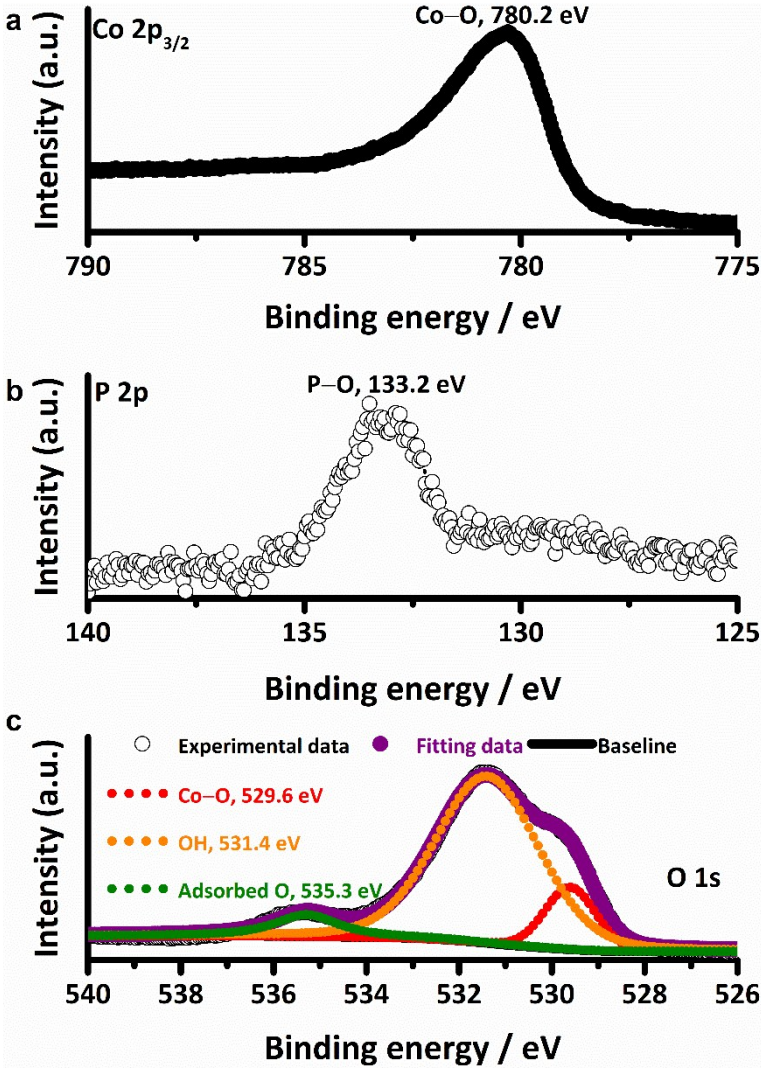

Fig. S23. (a) Co $2p_{3/2}$, (b) P 2p and (c) O 1s XPS spectra of hollow CoP OCHs after 4000 CV cycles in 1.0 M KOH + 1.0 M methanol in the potential range of 0 – 0.35 V *vs.* SCE at 100 mV s^{-1}.

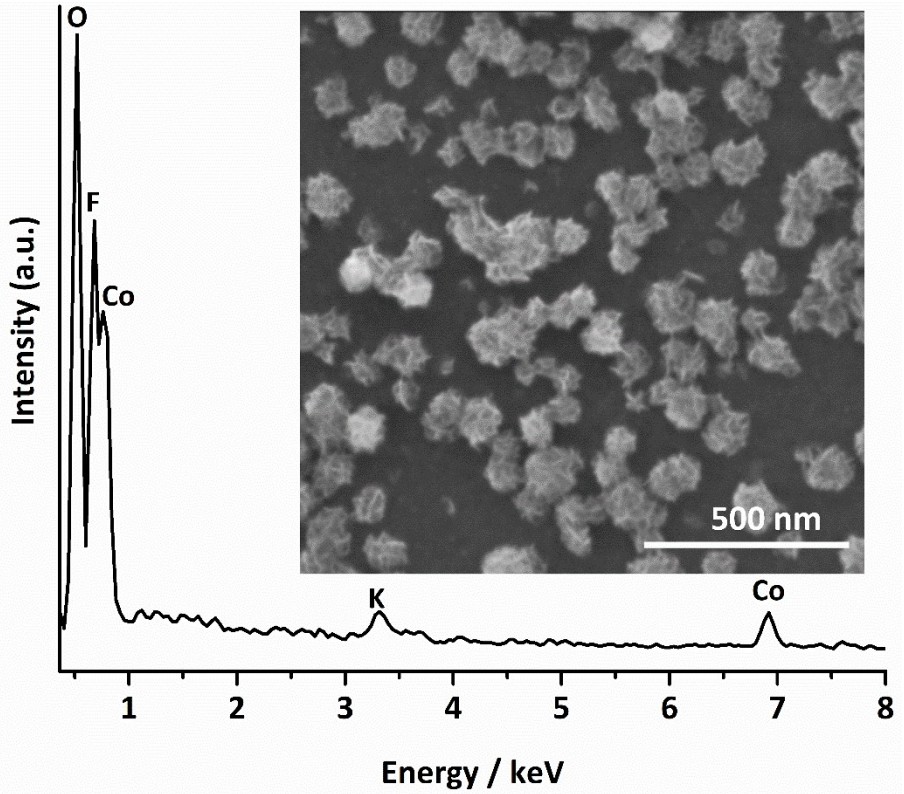

Fig. S24. SEM image and EDX spectrum of hollow CoP OCHs after 4000 CV cycles in 1.0 M KOH + 1.0 M methanol in the potential range of 0 – 0.35 V *vs.* SCE at 100 mV s^{-1}.

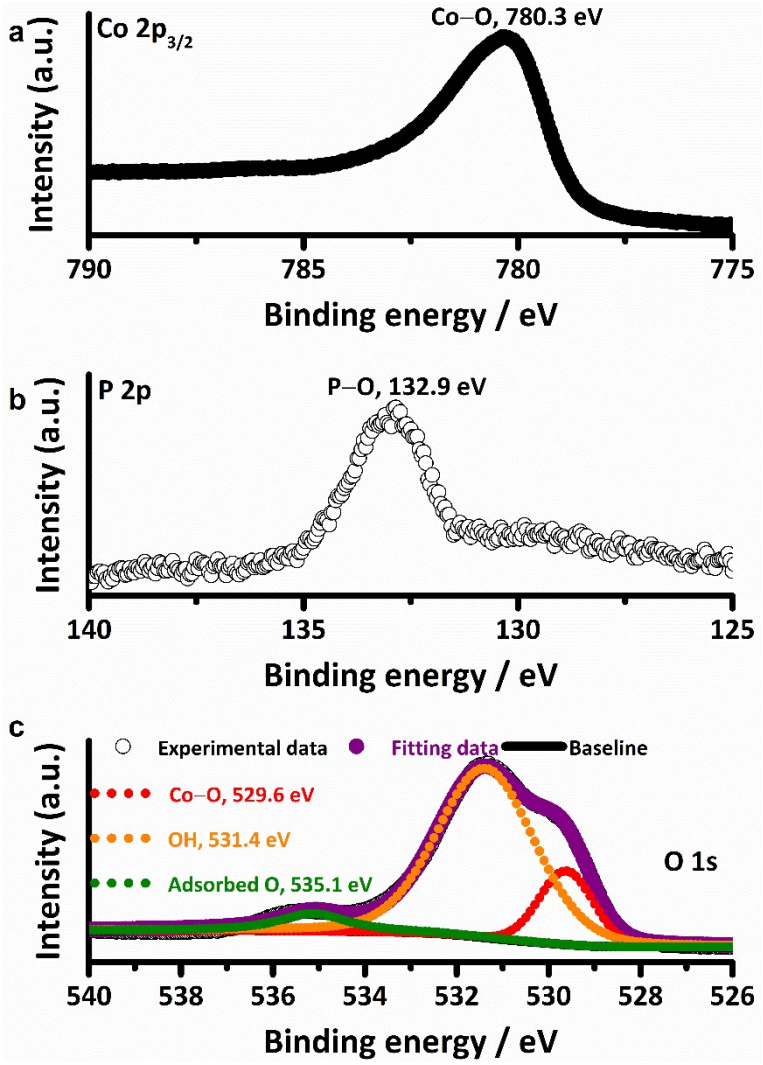

Fig. S25. (a) Co $2p_{3/2}$, (b) P 2p and (c) O 1s XPS spectra of porous CoP NSs after the OER test at 10 mA cm^{-2} for 60 h.

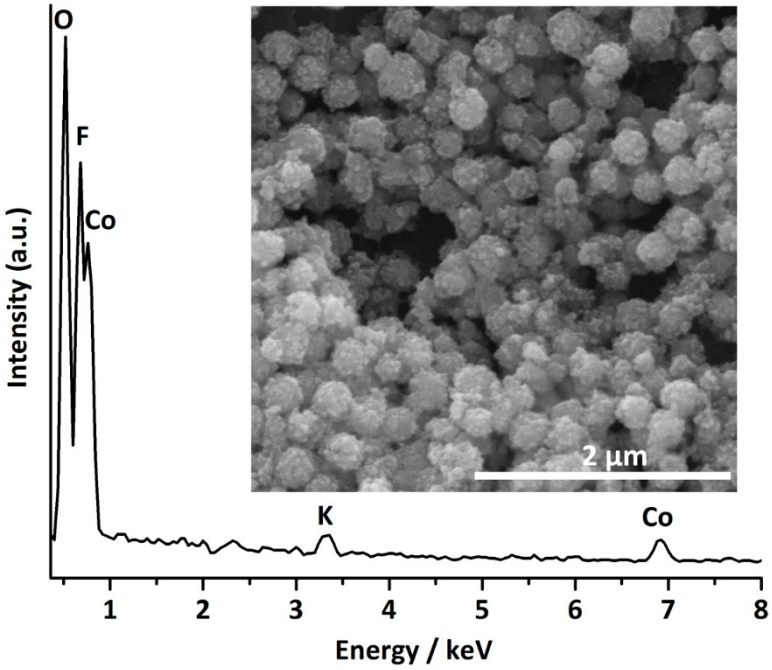

Fig. S26. SEM image and EDX spectrum of porous CoP NSs after the OER test at 10 mA cm^{-2} for 60 h.

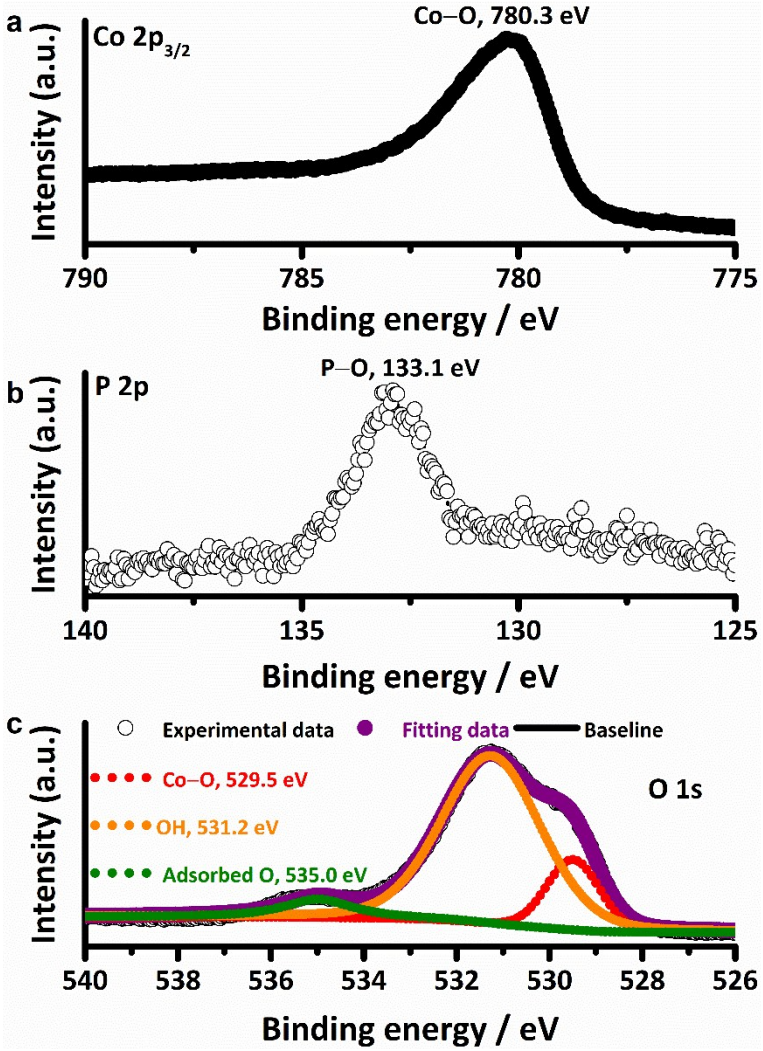

Fig. S27. (a) Co $2p_{3/2}$, (b) P 2p and (c) O 1s XPS spectra of porous CoP NSs after 4000 CV cycles in 1.0 M KOH + 1.0 M methanol in the potential range of 0 – 0.35 V *vs.* SCE at 100 mV s^{-1}.

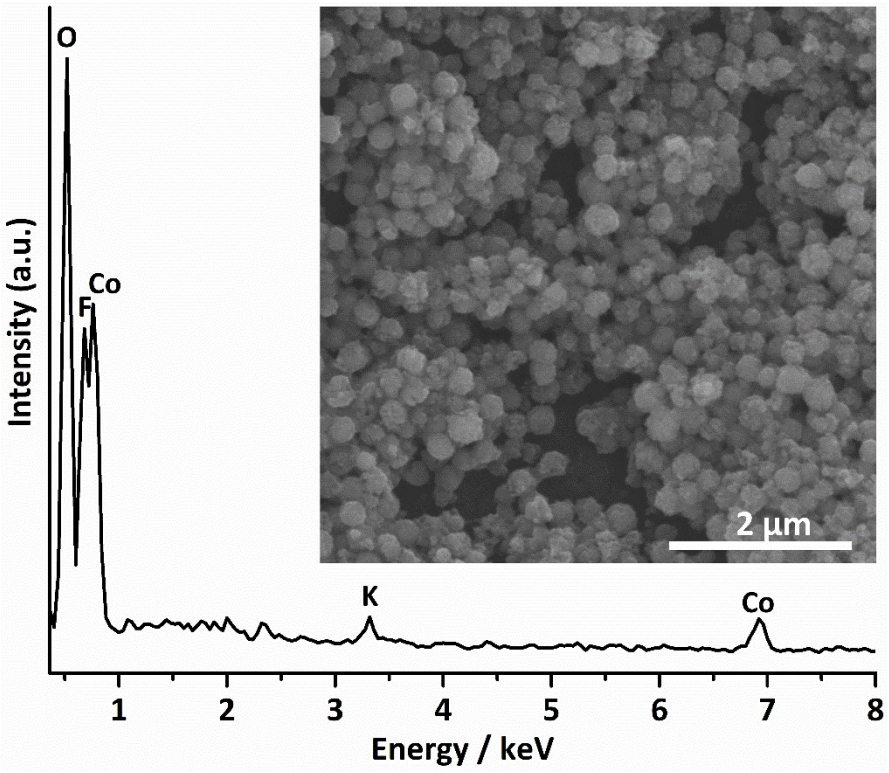

Fig. S28. SEM image and EDX spectrum of porous CoP NSs after 4000 CV cycles in 1.0 M KOH + 1.0 M methanol in the potential range of 0 – 0.35 V *vs.* SCE at 100 mV s^{-1}.

Table S1. Comparison of the OER performance of hollow CoP OCHs with those of other advanced OER catalysts tested in 1.0 M KOH electrolyte.

Catalysts	Substrate	Loading (mg cm^{-2})	η_{10} (mV)[a]	j_{300} (mA cm^{-2})[b]	Tafel slope (mV dec^{-1})	TOF_{300} (s^{-1})[c]	References
Hollow CoP OCHs	**Carbon paper**	**0.50**	**240**	**155**	**38**	**0.072**	**This work**
Porous CoP NSs	**Carbon paper**	**0.50**	**280**	**22**	**45**	**0.01**	**This work**
$Fe_{10}Co_{40}Ni_{40}P$ nanosheet	Glassy carbon	3.10	250	ca.105	44	ca. 0.007	*RSC Adv.* **2016**, *6*, 9647.
$Ni_{1.5}Fe_{0.5}P$ nanosheet	Carbon paper	1.38	264	ca.112	55	ca. 0.014	*Nano Energy* **2017**, *34*, 472.
$Co_{0.7}Fe_{0.3}P$/CNT nanoparticle	Carbon paper	0.50	243	/	36	/	*Adv. Funct. Mater.* **2017**, *27*, 1606635.
$Fe_{1.1}Mn_{0.9}P$ nanorod	Glassy carbon	0.284	440	/	39	/	*Chem. Mater.* **2017**, *29*, 3048.
Al-CoP nanoarray	Carbon cloth	5.7	265	ca. 50	51	ca. 0.0015	*Nanoscale* **2017**, *9*, 4793
FeCoP nanoarray	Ti foil	1.03	230	ca.90	67	ca. 0.013	*Adv. Mater.* **2017**, *29*, 1602441.
Co_4Ni_1P nanotube	Rotating disk electrode	0.19	245	ca. 20	61	0.032	*Adv. Funct. Mater.* **2017**, *27,* 1703455.
Fe-Ni-P/rGO nanoparticle	Rotating disk electrode	0.30	240	ca. 40	63	ca. 0.048	*ACS Appl. Mater. Interfaces* **2017**, *9*, 23852
NiCoP/C nanobox	Glassy carbon	ca. 0.25	330	< 5	96	< 0.004	*Angew. Chem. Int. Ed.* **2017**, *56*, 3897.
h-CoNiP/rGO nanoparticle	Glassy carbon	0.21	280	< 20	65.2		*Electrochem. Commun.* **2017**, *83*, 85
NiCoP/NC PHC nanoparticle	Rotating disk electrode	0.28	297	ca. 10	51		*J. Mater. Chem. A* **2017**, *5,* 18839
$(Ni_xFe_{1-x})_2P$ hollow nanocubes	Glassy carbon	0.30	290	ca.12	44	ca. 0.008	*Catal. Sci. Technol.* **2017**, *7*, 1549
N doped C/Ni_5P_4/Fe_3P hollow nanocube	Graphite electrode	0.50	252	ca. 40	24	ca. 0.016	*J. Mater. Chem. A* **2017**, *5*, 19656
Co-Fe-P nanoparticle	Ni foam	1.0	244	ca. 50	58	ca. 0.01	*ACS Appl. Mater. Interfaces*, **2017**, *9*, 362.
CoNiP nanoparticle	Glassy carbon	0.210	375	< 2	76	< 0.002	*Electrochem. Commun.* **2017**, *79,* 41.
NiCoP nanoplate	Ni foam	1.60	280	ca. 35	87	3.88[d]	*Nano Lett.* **2016**, *16,* 7718.
Mesoporous Co_3Ni_1P	Rotating disk electrode	ca. 0.20	280	ca.15	66.50	ca. 0.050	*ACS Energy Lett.* **2016**, *1*, 792.
O-CoP/GO nanoparticle	Glassy carbon	0.28	280	ca. 14	75	0.01	*J. Am. Chem. Soc.* **2016**, *138*, 14686.
Nanoporous $(Co_{0.52}Fe_{0.48})_2P$	CoFe ribbon	/	270	ca. 95	30	/	*Energy Environ. Sci.* **2016**, *9*, 2257.
NiCoP/RGO nanoparticle	Carbon paper	0.15	270	ca. 20	65.7	ca. 0.047	*Adv. Funct. Mater.* **2016**, *26*, 6785.
$Ni_{0.51}Co_{0.49}P$ film	Ni foam	/	239	ca. 80	45	/	*Adv. Funct. Mater.* **2016**, *26*, 7644.
NiCoP nanosheet array	Ni foam	/	/	ca. 50	/	/	*Nano Res.* **2016**, *9*, 2251.
CoMnP nanoparticle	Glassy carbon	0.284	330	ca. 5	61	ca. 0.004	*J. Am. Chem. Soc.* **2016**, *138*, 4006.
$(Co_{0.54}Fe_{0.46})_2P$ nanoparticle	Glassy carbon	0.20	370	< 1	/	< 0.001	*Angew. Chem. Int. Ed.* **2015**, *54,* 9642.
Amorphous Co-Fe-P nanosphere	Carbon paper	0.20	217		40		*J. Mater. Chem. A* **2017**, *5*, 25378.
Ni-Co-P nanosphere	Carbon paper	3.5	310	ca. 7	70	ca. 0.00046	*Nanoscale* **2016**, *8*, 19129
FeP nanotube	Carbon cloth	/	288	ca. 18	43	/	*Chem. Eur. J.* **2015**, *21*, 18062.
FeP nanorod	Carbon paper	0.70	350	< 5	63.6	ca. 0.002	*Chem. Commun.* **2016**, *52,* 8711.
FeP−FeP_xO_y nanotube	Glassy carbon	0.30	280	ca. 23	48	ca. 0.02	*ACS Appl. Nano Mater.* **2018**, *1*, 617
CoP nanopatirlce	Glassy carbon	ca. 0.40	310	ca. 9	70	/	*J. Am. Chem. Soc.* **2018**, *140*, 2610
CoP film	Cu foil	/	345	< 5	47	/	*Angew. Chem. Int.Ed.*

CoP mesoporous nanorod array	Ni foam	/	290	ca. 30	65	/	**2015**, *54,* 6251. *Adv. Funct. Mater.* **2015**, *25*, 7337.
CoP nanorod	Glassy carbon	0.71	320	ca. 5	71	ca. 0.002	*ACS Catal.* **2015**, *5,* 6874.
CoP nanowire	Co foam	/	248	100	78	/	*Chem. Sci.* **2017**, *8*, 2952.
CoP_3 nanosphere	Carbon cloth		291	ca. 12	72		*J ALLOY COMPD.* **2017**, *729*, 203
Co-P nanosphere	FTO		420	< 5	83		*RSC Adv.* **2016**, *6*, 52761
Porous urchin-Like Ni_2P	Ni foam	/	200	ca. 120	/	ca. 0.003	*ACS Catal.* **2016**, *6*, 714.
Carbon coated porous Ni-P nanoplate	Rotating disk electrode	0.20	300	10	64	ca. 0.010	*Energy Environ. Sci.* **2016**, *9*, 1246.
N_2P nanowire	Glassy carbon	0.14	290	ca. 15	47	ca. 0.021	*Energy Environ. Sci.* **2015**, *8,* 2347
Ni_2P	Carbon paper	1.33	280	ca. 24	48	ca. 0.007	*ACS Catal.* **2017**, *7*, 5450
CoO_x@CN nanoparticle	Ni foam	2.10	260	ca. 20	/	ca. 0.002	*J. Am. Chem. Soc.* **2015**, *137,* 2688.
Porous MoO_2 nanosheet	Ni foam	2.90	260	ca. 30	/	ca. 0.0025	*Adv. Mater.* **2016**, *28*, 3785.
$Ni_{0.75}V_{0.25}$-LDH nanosheet	Glassy carbon	0.143	300	10	50	ca. 0.0216	*Nat. Commun.* **2016**, *7,* 11981.
VOOH Hollow NS	Ni foam	0.80	270	ca. 25	68	ca. 0.006	*Angew. Chem. Int. Ed.* **2017**, *56*, 573.
Ni_3C/C nanoparticle	Carbon paper	0.285	ca. 310		46	ca. 0.009	*Adv. Mater.* **2016**, *28,* 3326.
Fe-Ni_3C nanodot	Glassy carbon	0.153	275	ca.20	62	ca. 0.02	*Angew. Chem. Int. Ed.* **2017**, *56,* 12566.
Ni_3S_2 nanosheet array	Ni foam	1.60	260	ca. 20	/	ca. 0.003	*J. Am. Chem. Soc.* **2015**, *137,* 14023.
Co_3Se_4 Nanowire	Co foam	2.60	/	161.7	44	0.026	*Adv. Energy Mater.* **2017**, *7*, 1602579.
Ni_3FeN nanoparticle	Glassy carbon	0.35	280	ca. 20	46	ca. 0.009	*Adv. Energy Mater.* **2016**, *6*, 1502585.
Three-Dimensional nanoporous iron nitride Film	Ni foam	/	238	ca. 100	44.5	/	*ACS Catal.* **2017**, *7,* 2052.

[a] The overpotential at the current density of 10 mA cm^{-2}.
[b] The current density at the overpotential of 300 mV.
[c] The TOF value at the overpotential of 300 mV based on the mass of the loaded catalysts.
[d] The TOF was calculated based on the surface active site, not the mass of the loaded catalysts.

Table S2. Comparison of the MOR performance of hollow CoP OCHs with those of other MOR catalysts reported in the literature.

Catalysts	Substrate	Loading (mg cm^{-2})	Electrolyte	Scan rate (mV s^{-1})	Onset potential (V *vs.* SCE)	Potential@ 50 mA cm^{-2} (V *vs.* SCE)	References
Hollow CoP OCHs	**Carbon paper**	**0.50**	**1.0 M KOH+1.0 M methanol**	**5**	**0.23**	**0.35**	**This work**
Porous CoP NSs	**Carbon paper**	**0.50**	**1.0 M KOH+1.0 M methanol**	**5**	**0.26**	**0.43**	**This work**
NiSe nanowire	Ni foam		1.0 M KOH+1.0 M methanol	10	ca. 0.30	ca. 0.40	*RSC Adv.* **2015**, *5*, 87051.
CoP array	Carbon cloth	1.47	1.0 M KOH+1.0 M methanol	10	ca. 0.23	ca. 0.40	*Nanotechnology* **2016**, *27*, 44LT02.
Ni-Co-O oxides			1.0 M KOH+1.0 M methanol	50	ca. 0.30	ca. 0.60	*Mater. Lett.* **2017**, *196*, 365.
Co_3O_4@CoP	Ni foil	1.0	1.0 M KOH+1.0 M methanol	10	ca. 0.25	> 0.50	*Adv. Energy Mater.* **2017**, *7*, 1602643.
$Co(OH)_2$ nanoflakes	Ni foam	0.50	1.0 M KOH+0.5 M methanol	10	0.27	ca. 0.40	*New J. Chem.* **2017**, *41*, 9546.
Co_2P@Co/N-C nanoparticle	Rotating disk electrode	0.20	1.0 M KOH+0.5 M methanol	10	0.30	>> 0.50	*Small* **2017**, *13*, 1700796.
$Cu(OH)_2$ @CCHH nanowire	Copper foam	15	1.0 M KOH+0.5 M methanol	10	ca. 0.20	ca. 0.33	*Small* **2017**, *13*, 1602755.
Ni-NiO@C nanoparticle	Glassy carbon	0.36	1.0 M KOH+0.5 M methanol	50	ca. 0.30	ca. 0.60	*J. Phys. Chem. Solids* **2018**, *112*, 119.

Note: The MOR performance is highly dependent on the test conditions, including electrolyte (concentration of KOH or/ and methanol) and CV scan rate, for the same catalyst. Therefore, only some representative transition metal based catalysts tested under similar conditions are listed here.

References

[S1] H. Liu, F. X. Ma, C. Y. Xu, L. Yang, Y. Du, P. P. Wang, S. Yang and L. Zhen, *ACS Appl. Mater. Interfaces,* 2017, **9**, 11634.

[S2] C. C. L. McCrory, S. Jung, I. M. Ferrer, S. M. Chatman, J. C. Peters and T. F. Jaramillo, *J. Am. Chem. Soc.,* 2015, **137**, 4347.

[S3] J. Y. Xu, J. J. Li, D. H. Xiong, B. S. Zhang, Y. F. Liu, K. H. Wu, I. Amorim, W. Li and L. F. Liu, *Chem. Sci.,* 2018, **9***,* 3470.

[S4] D. Meki, S. Fierro, H. Vrubel and X. L. Hu, *Chem. Sci.,* 2011, **2**, 1262.

[S5] J. Y. Xu, T. F. Liu, J. J. Li, B. Li, Y. F. Liu, B. S. Zhang, D. H. Xiong, I. Amorim, W. Li and L. F. Liu, *Energy Environ. Sci.,* 2018, 10.1039/C7EE03603E.

[S6] Y. P. Zhu, Y. P. Liu, T. Z. Ren and Z. Y. Yuan, *Adv. Funct. Mater.,* 2015, **25**, 7337.

[S7] J. F. Chang, Y. Xiao, M. L. Xiao, J. J. Ge, C. P. Liu and W. Xing, *ACS Catal.,* 2015, **5**, 6874.

[S8] W. Li, X. F. Gao, D. H. Xiong, F. Xia, J. Liu, W. G. Song, J .Y. Xu, S. M . Thalluri, M. F. Cerqueira, X. L. Fu and L. F. Liu, *Chem. Sci.,* 2017, **8**, 2952.

[S9] D. Li, H. Baydoun, C. N. Vernai and S. L. Brock, *J. Am. Chem. Soc.,* 2016, **138**, 4006.

[S10] H. F. Liang, A. N. Gandi, D. H. Anjum, X. B. Wang, U. Schwingenschlögl and H. N. Alshareef, *Nano Lett.,* 2016, **16**, 7718.

[S11] N. Jiang, B. You, M. L. Sheng and Y. J. Sun, *Angew. Chem. Int. Ed.,* 2015, **54**, 6251.